


Giant coercivity, resistivity upturn, and anomalous Hall effect in ferrimagnetic FeTbLijun Zhu ^{1,2,*}, Lujun Zhu,³ Qianbiao Liu,¹ and Xin Lin^{1,2}¹State Key Laboratory of Superlattices and Microstructures, Institute of Semiconductors, Chinese Academy of Sciences, Beijing 100083, China²College of Materials Science and Opto-Electronic Technology, University of Chinese Academy of Sciences, Beijing 100049, China³College of Physics and Information Technology, Shaanxi Normal University, Xi'an 710062, China

(Received 20 April 2023; revised 20 June 2023; accepted 1 July 2023; published 17 July 2023)

Despite the blooming interest, the transition-metal rare-earth ferrimagnets have not been comprehensively understood in terms of their coercivity and transport properties. Here, we report a systematic study of the magnetic and transport properties of ferrimagnetic FeTb alloy by varying the layer thickness and temperature. The FeTb is tuned from the Tb-dominated regime to the Fe-dominated regime via the layer thickness, without varying the composition. The coercivity closely follows the $1/\cos\theta_H$ scaling (where θ_H is the polar angle of the external magnetic field) and increases quasiexponentially upon cooling (exceeding 90 kOe at low temperatures), revealing that the nature of the coercivity is the thermally assisted domain-wall depinning field. The resistivity exhibits a quasilinear upturn upon cooling possibly due to thermal vibrations of the structure factor of the amorphous alloy. The existing scaling laws of the anomalous Hall effect in the literature break down for the amorphous FeTb that are either Fe or Tb dominated. These findings should advance the understanding of the transition-metal-rare-earth ferrimagnets and the associated ferrimagnetic phenomena in spintronics.

DOI: [10.1103/PhysRevB.108.014420](https://doi.org/10.1103/PhysRevB.108.014420)**I. INTRODUCTION**

Ferrimagnetic materials (FIMs), which have two antiferromagnetically coupled sublattices, are of considerable interest in the field of spintronics [1–5]. FIMs are potentially advantageous for dense magnetic recording applications [6] because of their tunable magnetism, less sensitivity to stray magnetic fields than ferromagnets (FMs), and easier and fast detection than antiferromagnets (AFMs). Moreover, FIMs are an exotic platform to study the interplay of spin-orbit physics and AFM coupling as a function of the degree of magnetic compensation. Several striking spin-orbit coupling (SOC) phenomena have been demonstrated to arise from the magnetization compensation within the bulk of the FIMs, such as large magnetic domain-wall velocities near compensation [3–5], strong compensation dependence and sign reversal of bulk spin-orbit torques (SOTs) [7], strong variation of the “interfacial” SOTs with the relative spin-relaxation rates within the bulk of FIMs [8,9], and lack of current-driven magnetization switching at full magnetization compensation [10–12]. However, the spin-mixing conductance of the interfaces of metallic FIMs is insensitive to temperature, magnetic compensation or the areal density of the magnetic moment of the interface [8], in contrast to the insulating FIM case [13,14].

An in-depth understanding of the ferrimagnetic phenomena in magnetic heterostructures requires insights into the mechanisms of the coercivity (H_c), the electron momentum scattering, and the anomalous Hall effect (AHE) of the FIMs. Note that the coercivity of a perpendicular magnetization represents the switching barrier to overcome by the driving

magnetic field or SOT [15–17], while electron momentum scattering affects the generation [18–20] and relaxation of spin current via SOC [8,21,22]. The AHE typically functions as the indicator of the magnetization orientation in a variety of experiments (e.g., harmonic Hall voltages [7–9] and magnetization switching [14,15,19,23,24]). However, the magnetization of transition-metal rare-earth FIMs arises from two competing sublattices that have been suggested to contribute to the AHE in distinct manners (i.e., the $3d$ states of the transition metal governed the transport properties, while the $4f$ states of Tb were less involved [23,25,26]). The scaling behavior of the AHE in such transition-metal rare-earth FIMs thus becomes stimulating open questions.

In this work, we systematically examine the magnetic and transport properties of FeTb, a representative FIM, as a function of layer thickness and temperature. We show that the coercivity can be rather high and increase quasiexponentially upon cooling due to the nature of the thermally assisted domain-wall depinning field. The large longitudinal resistivity (ρ_{xx}) increases quasilinearly upon cooling. The anomalous Hall resistivity (ρ_{AH}) cannot be described by the existing scaling laws [27–29].

II. SAMPLES AND MAGNETIZATION

For this work, we deposit four FeTb films with different thicknesses ($t = 8, 16, 32, \text{ and } 48 \text{ nm}$) on Si/SiO₂ substrates by cosputtering at room temperature. Each sample is capped by a MgO (2 nm)/Ta (2 nm) bilayer that is fully oxidized upon exposure to the atmosphere. The composition of all the FeTb layers is Fe_{0.55}Tb_{0.45} in volume percentage as calibrated using the deposition rates of the Fe and the Tb. This composition corresponds to a Tb/Fe atomic ratio of ≈ 0.3 (as calculated

*ljzhu@semi.ac.cn

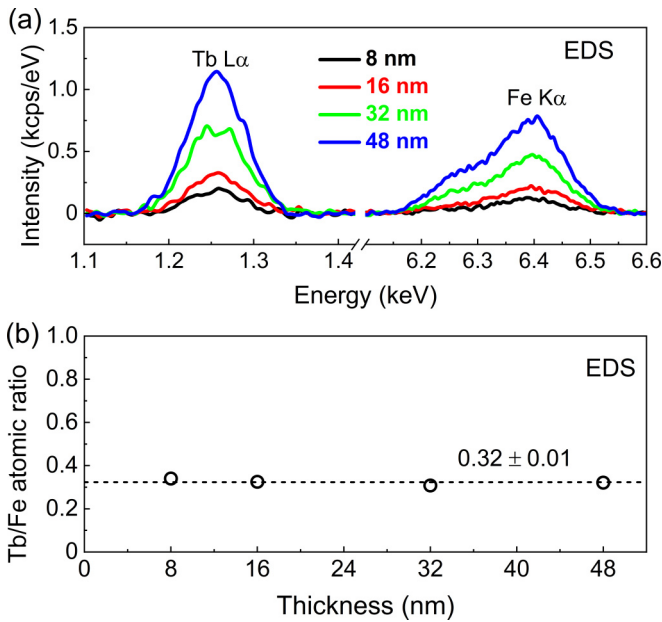


FIG. 1. (a) Energy-dispersive spectra collected using a Bruker EDS tool and (b) Tb/Fe atomic ratio calculated using Tb $L\alpha$ and Fe $K\alpha$ EDS spectra for FeTb films with different thicknesses, revealing that composition is same for FeTb films studied in this work.

using the atomic volumes of bulk Fe and Tb crystals), which is consistent with the energy-dispersive spectroscopy (EDS) results (0.32 ± 0.01) in Figs. 1(a) and 1(b). Such FeTb films are amorphous and homogeneous as indicated by scanning

transmission electron microscopy and electron-energy-loss spectra results of the samples prepared by the same sputtering tool using similar parameters within the same few days [7].

The saturation magnetization (M_s) for each FeTb film, the sum contribution of the Fe and the Tb sublattices [Fig. 2(a)], is measured using a superconducting quantum interference device. Figure 2(b) shows the temperature profile of the saturation magnetization of the FeTb films with different thicknesses. M_s for the 8-nm FeTb varies nonmonotonically with temperature and peaks at 250 K. For the 16-nm FeTb, M_s increases monotonically from being negligibly small at temperatures below 50 K to ≈ 60 emu/cm 3 as the temperature approaches 300 K. In contrast, for both the 32- and 48-nm FeTb, M_s decreases first slowly and then more rapidly as the temperature increases. The diverse temperature profiles of the saturation magnetization of the FeTb films imply a strong tuning of the magnetization compensation configuration by thickness. As plotted in Fig. 2(b), the magnetization exhibits full compensation at the “compensation thickness” of 16 nm at 5 K and of ≈ 20 nm at 300 K. Thus, the magnetization compensation of the FeTb alloy is not only a function of substrate [7], composition [7,30,31], and strain [32], but also of temperature and thickness.

The films are then patterned into 5×60 - μm^2 Hall bars for electrical measurements using a physical properties measurement system (PPMS-9T). From the AHE measurements [see Figs. 2(c) and 2(d)], the FeTb films have fairly square hysteresis loops for the transverse resistivity (ρ_{xy}), implying good magnetic uniformity of these films. The polarity of the hysteresis loop is opposite for the 8- and 16-nm FeTb samples

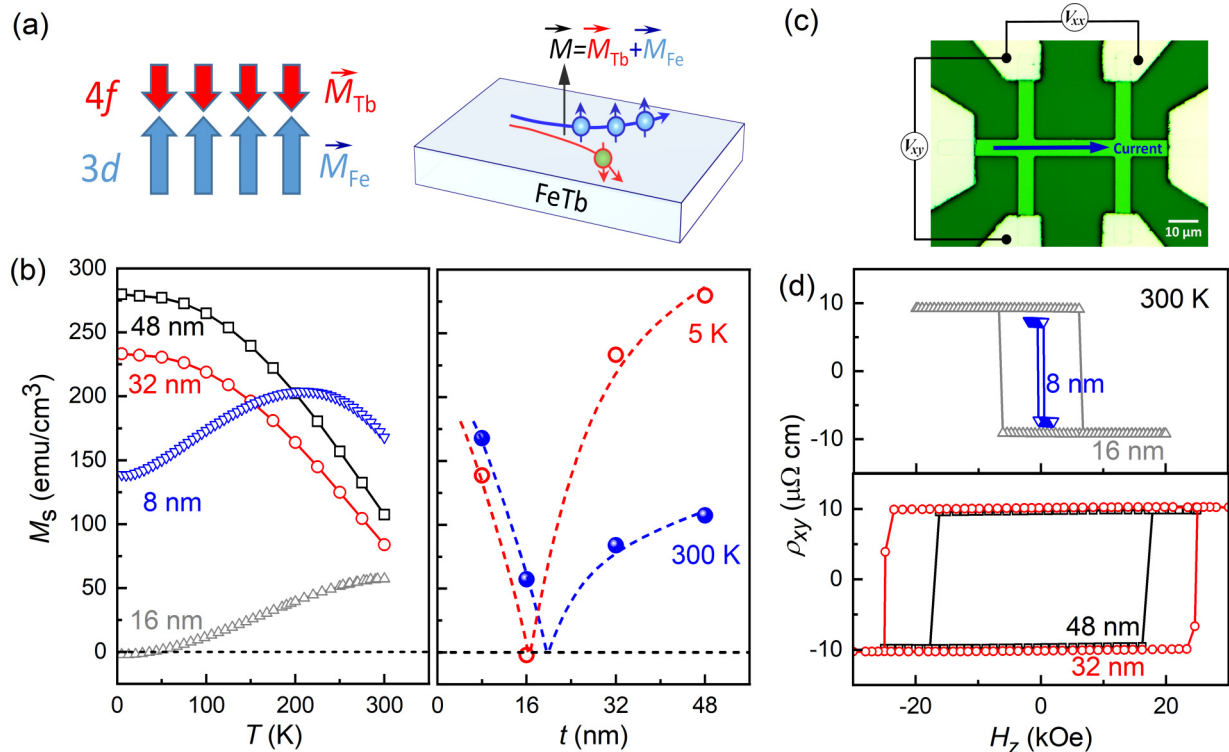


FIG. 2. (a) Schematic depiction of ferrimagnetism and anomalous Hall effect in FeTb. (b) Dependence of saturation magnetization on temperature, (c) Dependence of saturation magnetization on thickness at 5 and 300 K, and (d) Transverse resistivity at 300 K for FeTb with different layer thicknesses.

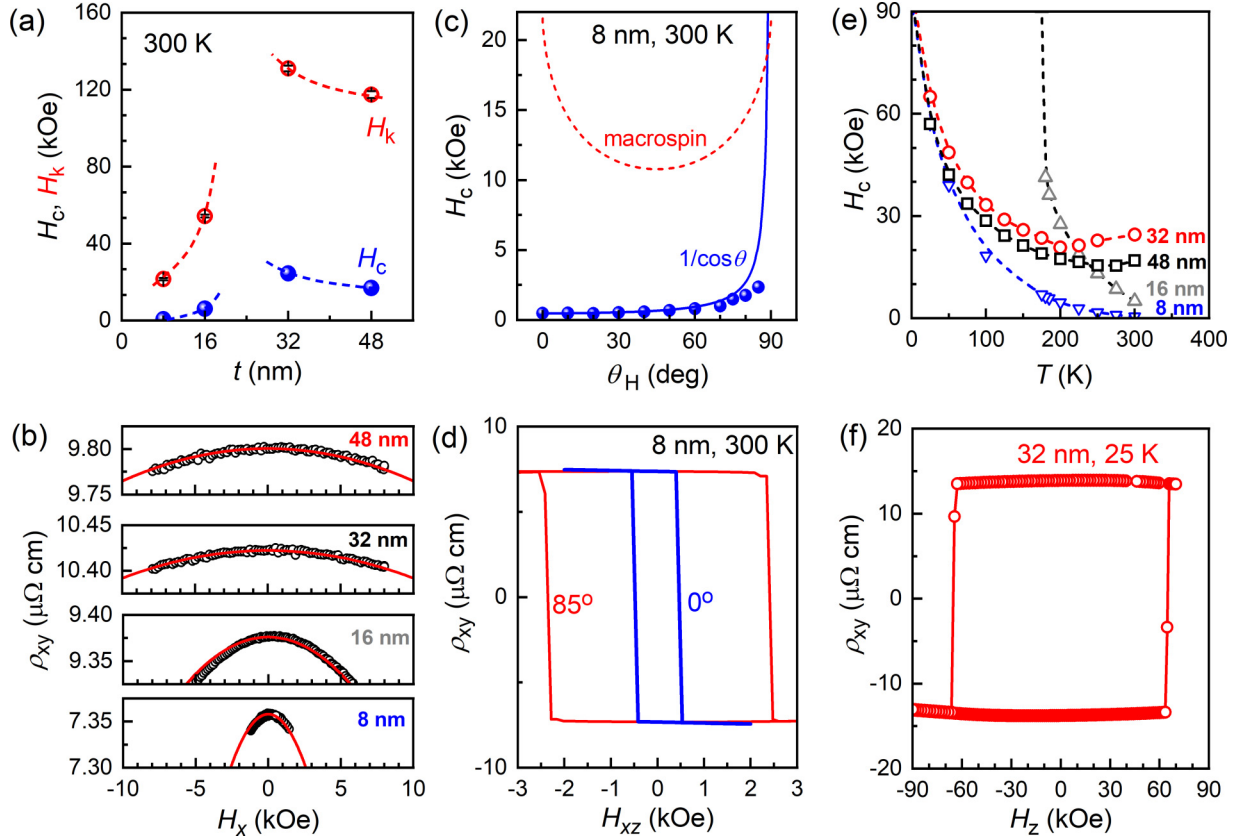


FIG. 3. (a) Perpendicular coercivity and perpendicular magnetic anisotropy field and (b) parabolic scaling of transverse resistivity with in-plane magnetic field for FeTb with different thicknesses (300 K). (c) Dependence on the polar angle (θ_H) of the room-temperature coercivity. (d) Transverse resistivity hysteresis loops for 8-nm FeTb measured at $\theta_H = 0^\circ$ and 85° and 300 K. (e) Dependence on temperature of perpendicular coercivity ($\theta_H = 90^\circ$) of FeTb films. (f) Transverse resistivity hysteresis loop at 25 K for 32-nm FeTb, displaying a giant coercivity of 65 kOe.

compared to that for the 32- and 48-nm ones, suggesting that the films are Tb dominated at 8 and 16 nm but Fe dominated at 32 and 48 nm. Such striking thickness dependences of the magnetization and the transverse resistivity are interesting observations and worth future investigation. While the unambiguous identification of the exact mechanism is beyond the scope of this paper, we speculate that the striking thickness dependence of the magnetic and transport properties might be related to some hidden short-range ordering within the amorphous films.

III. GIANT, STRONGLY TEMPERATURE-DEPENDENT COERCIVITY

Figure 3(a) shows the out-of-plane coercivity and the effective perpendicular magnetic anisotropy field (H_k) at 300 K. Here, the out-of-plane coercivity is estimated from the switching of the transverse resistivity by a perpendicular magnetic field [H_z , Fig. 2(d)], while H_k is estimated from the parabolic scaling of ρ_{xy} with the in-plane magnetic field (H_{xy}) due to tilting of the magnetization [Fig. 3(b)], i.e.,

$$\rho_{xy} = \rho_{AH} \cos(\arcsin(H_{xy}/H_k)) \approx \rho_{AH} [1 - 1/2(H_{xy}/H_k)^2]. \quad (1)$$

Both H_c and H_k vary as a function of the layer thickness and tend to increase upon approaching the compensation thickness. As shown in Figs. 3(c) and 3(d), H_c follows a $1/\cos\theta_H$

scaling (θ_H is the polar angle of the driving magnetic field H_{xz}) and is typically much smaller than the perpendicular magnetic anisotropy field at $\theta_H = 0^\circ$. This is in contrast to the case of a perpendicular macrospin, for which the coercivity varies as

$$H_c = H_k (\cos^{2/3} \theta_H + \sin^{2/3} \theta_H)^{-3/2}, \quad (2)$$

and is equal to H_k at $\theta_H = 0^\circ$ and 90° . As plotted in Fig. 3(e), the out-of-plane coercivity of each FeTb film increases upon cooling in a quasiexponential manner. These observations consistently reveal that the coercivity of the FeTb represents the thermally assisted depinning field of the magnetic domain walls rather than the bulk magnetic anisotropy field. This is generally the case for magnetic systems in which the reversed domain nucleation and domain-wall propagation (with the energy barrier of the domain-wall pinning field) require less energy than coherent rotation (with the energy barrier of H_k) [17].

We also note that the out-of-plane field required to switch these films, i.e., the coercivity, exceeds 90 kOe at temperatures below 175 K for the 16-nm FeTb and at temperatures below 25 K for the other three samples. The rapid increase of the coercivity upon cooling is distinct from the enhancement of coercivity at the magnetization compensation points [1–5,7,33] because it occurs in the whole temperature region, including the temperatures at which the magnetization is very high [Fig. 2(b)]. The giant coercivity and square hysteresis

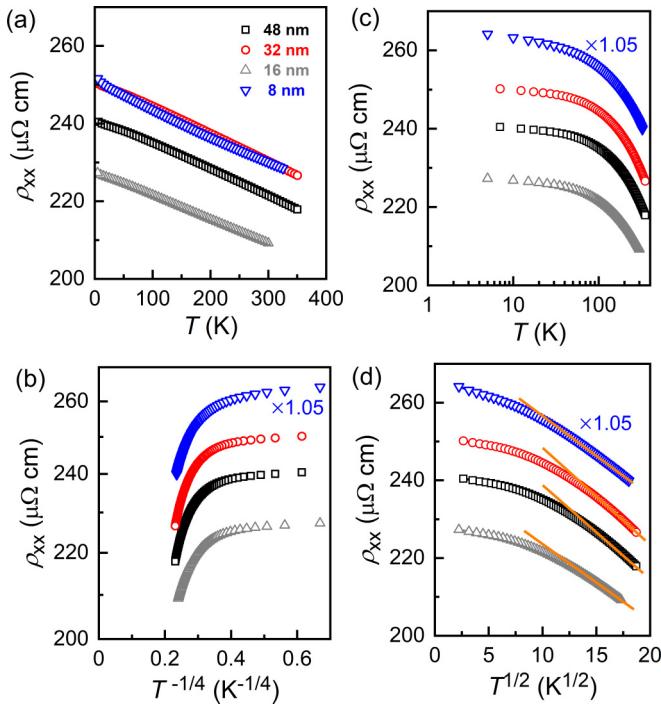


FIG. 4. Resistivities (ρ_{xx}) of FeTb films plotted as function of (a) temperature T , (b) T (in log plot), (c) $T^{-1/4}$, and (d) $T^{1/2}$. In (b)–(d) the resistivity data for 8-nm FeTb are multiplied by 1.05 for clarity. In (b) log plot of ρ_{FeTb} as function of $T^{-1/4}$ indicates lack of Mott’s law for hopping conduction; latter predicts $\ln \rho_{xx}$ to vary linearly with $T^{-1/4}$. In (d) straight lines represent best linear fits to data in high-temperature regime.

loops [Fig. 3(f)] may make these FeTb interesting hard magnets for some specific spintronic applications [34].

IV. RESISTIVITY UPTURN

Resistivity or electron momentum scattering is also a key property of a spintronic material. For instance, electron momentum scattering affects spin-dependent scattering, the generation and relaxation of spin current via SOC. To provide insight into the electron momentum scattering mechanism, we measure the resistivity of the FeTb samples as a function of temperature [Fig. 4(a)]. ρ_{xx} varies between 210 and 250 $\mu\Omega$ cm. In analogy to the magnetic properties and the anomalous Hall resistivity (see below), ρ_{xx} shows also an interesting nonmonotonic thickness dependence at each fixed temperature due to some exotic mechanism yet to be known. Here, interfacial scattering is unlikely to play any significant role in the determination of ρ_{xx} of these thick, resistive FeTb because they should have a very short mean-free path.

More interestingly, ρ_{xx} shows a quasilinear upturn upon cooling for each sample. Similar resistivity upturn has also been observed in 200-nm-thick FeTb films [35]. In general, a resistivity upturn can arise from weak localization, hopping conductance, orbital one-channel Kondo effect, orbital two-channel Kondo effect, electron-electron scattering, magnetic Brillouin-zone scattering, or scattering of electrons by thermal vibration of structure factor. However, none of these mechanisms appear to explain the resistivity upturn of these

FeTb films. First, weak localization, which diminishes under an external magnetic field or a strong internal exchange field, is not expected in the ferrimagnetic FeTb that have giant perpendicular magnetic anisotropy [Fig. 3(a)]. Hopping conductance is known to occur in Mott-Anderson insulators with extremely high resistivity (e.g., 10^6 – $10^9 \mu\Omega$ cm for quasicrystal AlPdRe [36], amorphous GeTe, and GeSb_2Te_4 annealed at 150 °C [37], 10^{11} – $10^{17} \mu\Omega$ cm for the Pt-SiO₂ granular film with Pt concentration of 0.11 [38,39]), but not in metals like FeTb with several orders of magnitude lower resistivity. The absence of hopping conductance is reaffirmed by the lack of a $T^{-1/4}$ scaling (so-called Mott’s law [40]) in the resistivity [Fig. 4(b)]. The orbital one-channel Kondo effect [41], if important, should increase the resistivity as a function of $\ln T$, which is not the case for the FeTb [Fig. 4(c)]. The resistivity upturn due to electron-electron interaction would follow a $T^{1/2}$ scaling at low temperatures [42], which is not consistent with the evident deviation from the $T^{1/2}$ scaling at temperatures below 150 K [Fig. 4(d)].

The orbital two-channel Kondo effect [41,43–46] is also less likely to explain the resistivity upturn in the amorphous FeTb films. This is because it would imply a Kondo temperature of >300 K (below which the $T^{1/2}$ scaling emerges) and a deviation temperature of 150 K (below which the resistivity deviates from the $T^{1/2}$ scaling), both of which are surprisingly high. Note that the Kondo temperature is only 23 K for the $L1_0$ -MnAl [42] and 14.5 K for $L1_0$ -MnGa films [45], a few degrees Kelvin for glasslike ThAsSe [43] and Cu point contacts [41], while the deviation temperature is typically below 1 K for all the previously studied two-channel Kondo systems [41–43].

Another possible mechanism for a resistivity upturn is the magnetic Brillouin-zone scattering (the periodic potentials due to antiferromagnetic alignment of the magnetic sublattices can produce an additional magnetic Brillouin zone, of smaller volume in k space than the ordinary lattice potential, whose planes further incise and contort the Fermi surface [47]). While this possibility cannot be quantitatively tested due to a lack of knowledge about the exact functional dependence on temperature, magnetic Brillouin-zone scattering should be weak in the amorphous FeTb which has no long-range periodicity in the crystalline and magnetic lattices. The resistivity upturn is also absent in epitaxial ferrimagnets of $\text{Mn}_{1.5}\text{Ga}$ [28] and Mn_2Ga [48] in which the two Mn sublattices are also AFM coupled.

After we have excluded any important role of weak localization, hopping conductance, orbital one-channel Kondo effect, orbital two-channel Kondo effect, electron-electron scattering, and magnetic Brillouin-zone scattering, scattering of electrons by thermal vibrations of the structure factor [49,50] is left as the most likely mechanism for the increase of resistivity with decreasing temperature over a wide range of temperature in our amorphous FeTb films. Thermal vibrations of the structure factor have been reported to explain the resistivity upturn in many liquid transition metals and metallic glass alloys [35,49,50]. Note that such thermal vibrations of the structure factor in disordered alloys are distinct from the phonon scattering that increases the resistivity with increasing temperature in ordered crystalline materials [27–29,44]. Future theoretical calculations of the structure factor as a

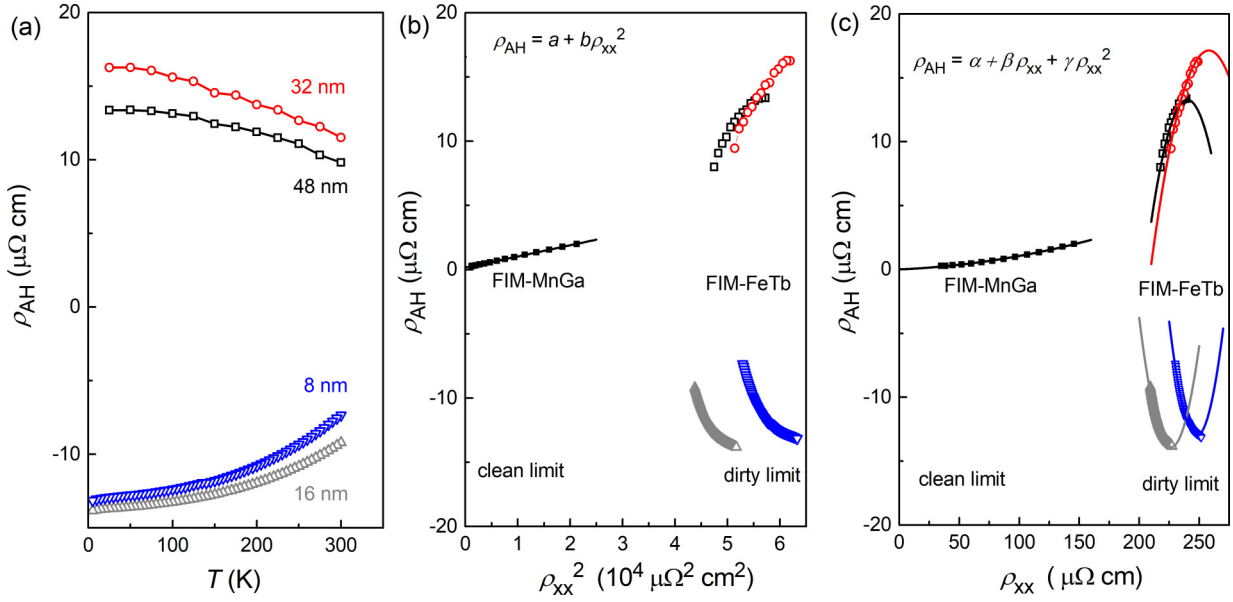


FIG. 5. Scaling of anomalous Hall effect. (a) Dependence on temperature of ρ_{AH} of FeTb films with different thicknesses. (b) ρ_{AH} vs ρ_{xx}^2 and (c) ρ_{AH} vs ρ_{xx} for FeTb films and control $Mn_{1.5}Ga$ sample. Solid straight lines in (b) represent fits of data to Eq. (3) and solid curves in (c) represent fits of data to Eq. (6).

function of temperature would be informative for a more quantitatively understanding of the resistivity of the FeTb samples, which is, however, beyond the scope of this paper.

V. SCALING OF THE STRONG ANOMALOUS HALL EFFECT

We now discuss the scaling of the anomalous Hall resistivity (ρ_{AH}) with the longitudinal resistivity (ρ_{xx}). The scaling analysis is interesting as it can disentangle the intrinsic and extrinsic contributions of the anomalous Hall resistivity of magnetic materials in which the electron scattering is dominated by impurity and phonon scattering. In that case, ρ_{AH} of a given sample is simply a linear function of ρ_{xx}^2 , i.e.,

$$\rho_{AH} = \alpha \rho_{xx0} + \beta_0 \rho_{xx0}^2 + b \rho_{xx}^2, \quad (3)$$

where α , β_0 , ρ_{xx0} , and b are constant for a given sample and $a = \alpha \rho_{xx0} + \beta_0 \rho_{xx0}^2$ goes to zero when the residual resistivity ρ_{xx0} (due to static impurity scattering at low temperatures) is zero. Equation (3) describes the AHE scaling of epitaxial FIM $Mn_{1.5}Ga$ [28] and some other $3d$ ferromagnets. Hou *et al.* [29] also proposed a multivariable scaling relation for the AHE in magnetic materials in *very high-conductivity* regime by assuming two major competing scattering sources: i.e.,

$$\rho_{AH} = \alpha \rho_{xx0} + \beta_0 \rho_{xx0}^2 + \gamma_0 \rho_{xx0} \rho_{xxT} + \beta_1 \rho_{xxT}^2, \quad (4)$$

where ρ_{xx0} is also the residual resistivity and $\rho_{xxT} = \rho_{xx} - \rho_{xx0}$ is resistivity due to dynamic phonon scattering at high temperatures; α , β_0 , γ_0 , and β_1 are fitting parameters. Equation (4) describes well the AHE scaling in epitaxial ferromagnetic Fe [27] grown by molecular-beam epitaxy. For convenience, we rewrite Eq. (4) as

$$\rho_{AH} = \alpha \rho_{xx0} + (\gamma_0 - 2\beta_1) \rho_{xx0} \rho_{xx} + (\beta_0 + \beta_1 - \gamma_0) \rho_{xx0}^2 + \beta_1 \rho_{xx}^2. \quad (5)$$

We note that Eqs. (3)–(5) predict that ρ_{AH} is a monotonic function of ρ_{xx} and scales smoothly to zero at zero ρ_{xx} ($\rho_{xx0} = \rho_{xxT} = 0$).

In Fig. 5(a), we plot the values of ρ_{AH} for the FIM FeTb as a function of temperature. While the anomalous Hall resistivities of the Fe-dominated and Tb-dominated films are of opposite signs, the magnitude increases monotonically, by 50%, for each sample. A similar increase of ρ_{AH} with temperature has also been reported in ferromagnetic MnAl with orbital two-channel Kondo effect [51] and is distinct from that of FMs (e.g., Fe [27], Co [52], Ni [53], and FePt [54]) and FIMs (MnGa [28]), in which the electron scattering is dominated by impurity scattering and phonon scattering. More surprisingly, ρ_{AH} of the FeTb is not a linear function of ρ_{xx}^2 and even does not have an obvious monotonic scaling towards zero as ρ_{xx} decreases. This observation suggests the breakdown of the conventional AHE scaling for the dirty metal of amorphous FeTb ferrimagnets. This breakdown is not a general case for FIMs as the $Mn_{1.5}Ga$ with AFM-coupled Mn sublattices does follow Eq. (3) [see Fig. 4(b)].

We show in Fig. 5(c) that the anomalous Hall resistivity phenomenally follows the law

$$\rho_{AH} = \alpha + \beta \rho_{xx} + \gamma \rho_{xx}^2, \quad (6)$$

where α , β , and γ are nonzero constants. Equation (6) predicts a peak and decay in ρ_{AH} at very high resistivities which might be consistent with the expectation that ρ_{AH} should reduce towards zero in the limit of infinite ρ_{xx} (insulators). Note that we have tested that the data in Fig. 5(c) cannot be fit by a monotonically varying exponential, logarithm, hyperbola, and other functions. The underlying physics and the precise application regime of this scaling, Eq. (6), require theoretical and experimental investigations in the future and is beyond the scope of this work.

Finally, we mention that the anomalous Hall resistivity of the FeTb is giant compared to that of the $3d$ magnets Fe [27],

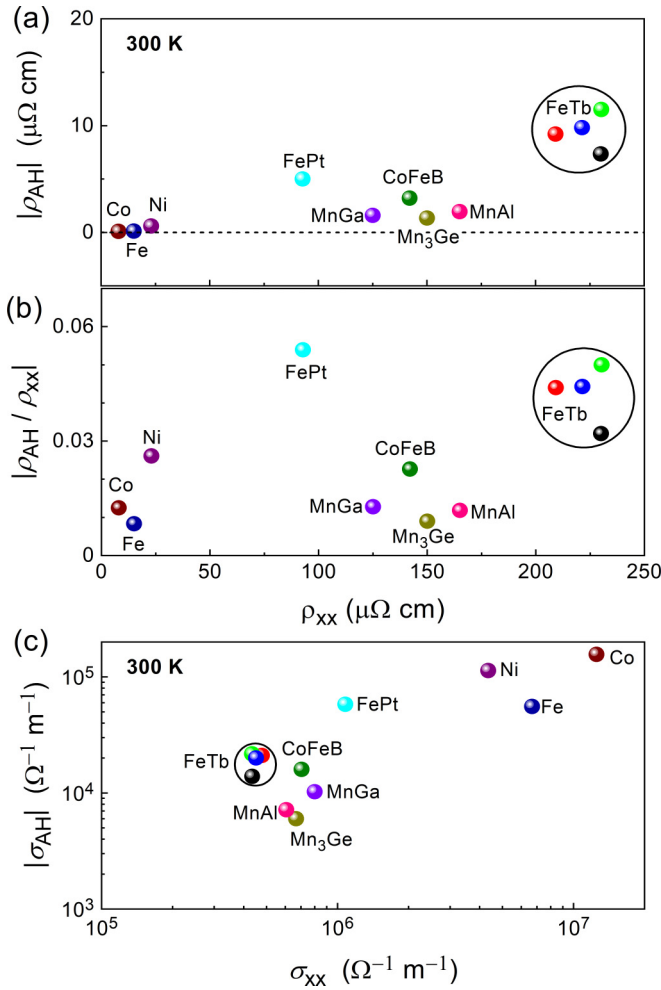


FIG. 6. Dependence on longitudinal resistivity of (a) anomalous Hall resistivity and (b) anomalous Hall angle of representative magnetic films. (c) Anomalous Hall conductivity of same materials plotted as function of longitudinal conductivity.

Co [52], Ni [53], Co₄₀Fe₄₀B₂₀ [55], Mn_{1.5}Ga [28], MnAl [51], and Mn₃Ge [56] [Fig. 6(a)] due to the large anomalous Hall angle $[\rho_{AH}/\rho_{xx}]$; see Fig. 6(b) and the high resistivity. As

plotted in Fig. 6(c), the anomalous Hall conductivity of the FeTb is also stronger than that of MnAl, MnGa, Mn₃Ge, and CoFeB with significantly higher longitudinal conductivities. Such giant anomalous Hall effect is highly preferred for sensor applications.

VI. CONCLUSION

We have presented a systematic study of the magnetic and transport properties of the ferrimagnetic FeTb alloy by varying the layer thickness and temperature. The FeTb is tuned from the Tb-dominated regime to the Fe-dominated regime simply via the increase of the layer thickness, without varying the composition. For each of the studied FeTb samples, the coercivity closely follows the $1/\cos\theta_H$ scaling (where θ_H is the polar angle of the external magnetic field) and increases quasiexponentially upon cooling and exceeds 90 kOe below a certain low temperature, revealing that the nature of the coercivity is thermally assisted domain-wall depinning field. The resistivity increases quasilinearly with temperature upon cooling likely due to thermal fluctuations of the structure factor of the amorphous FeTb. The anomalous Hall resistivities of both Fe- or Tb-dominated FeTb layers that are in the dirty limit cannot be described by any of the existing AHE scaling laws proposed in the literature. These exotic findings should advance the understanding of the magnetic and transport behaviors of the transition-metal rare-earth ferrimagnets.

ACKNOWLEDGMENTS

The authors thank Changmin Xiong for help with PPMS measurements. This work is supported partly by the National Key Research and Development Program of China (Grant No. 2022YFA1204004), partly by the National Natural Science Foundation of China (Grant No. 12274405), and partly by the Strategic Priority Research Program of the Chinese Academy of Sciences (Grant No. XDB44000000). The EDS measurements performed at Shaanxi Normal University was supported by the National Natural Science Foundation of China (Grant No. 51901121).

[1] N. Roschewsky, T. Matsumura, S. Cheema, F. Hellman, T. Kato, S. Iwata, and S. Salahuddin, Spin-orbit torques in ferrimagnetic GdFeCo alloys, *Appl. Phys. Lett.* **109**, 112403 (2016).
 [2] J. Finley, C. Lee, P. Y. Huang, and L. Liu, Spin-orbit torque switching in a nearly compensated Heusler ferrimagnet, *Adv. Mater.* **31**, 1805361 (2019).
 [3] K. Kim, S. K. Kim, Y. Hirata, S. Oh, T. Tono, D. Kim, T. Okuno, W. S. Ham, S. Kim, G. Go, Y. Tserkovnyak, A. Tsukamoto, T. Moriyama, K. Lee, and T. Ono, Fast domain wall motion in the vicinity of the angular momentum compensation temperature of ferrimagnets, *Nat. Mater.* **16**, 1187 (2017).
 [4] K. Cai, Z. Zhu, J. M. Lee, R. Mishra, L. Ren, S. D. Pollard, P. He, G. Liang, K. L. Teo, and H. Yang, Ultrafast and energy-efficient spin-orbit torque switching in compensated ferrimagnets, *Nat. Electron.* **3**, 37 (2020).

[5] L. Caretta, M. Mann, F. Büttner, K. Ueda, B. Pfau, C. M. Günther, P. Hessing, A. Churikova, C. Klose, M. Schneider, D. Engel, C. Marcus, D. Bono, K. Bagschik, S. Eisebitt, and G. S. D. Beach, Fast current-driven domain walls and small skyrmions in a compensated ferrimagnet, *Nat. Nanotechnol.* **13**, 1154 (2018).
 [6] F. Radu and J. Sánchez-Barriga, Ferrimagnetic heterostructures for applications in magnetic recording, in *In Advanced Nanomaterials, Novel Magnetic Nanostructures*, edited by N. Domracheva, M. Caporali, and E. Rentschler (Elsevier, Amsterdam, 2018), Chap. 9, pp. 267–331.
 [7] Q. Liu, L. Zhu, X. S. Zhang, D. A. Muller, and D. C. Ralph, Giant bulk spin-orbit torque and efficient electrical switching in single ferrimagnetic FeTb layers with strong perpendicular magnetic anisotropy, *Appl. Phys. Rev.* **9**, 021402 (2022).

- [8] L. Zhu and D. C. Ralph, Strong variation of spin-orbit torques with relative spin relaxation rates in ferrimagnets, *Nat. Commun.* **14**, 1778 (2023).
- [9] X. Lin, J. Li, L. Zhu, X. Xie, Q. Liu, D. Wei, G. Yuan, and L. Zhu, Strong enhancement of spin-orbit torques in ferrimagnetic $\text{Pt}_x(\text{Si}_3\text{N}_4)_{1-x}/\text{CoTb}$ bilayers by Si_3N_4 doping, *Phys. Rev. B* **106**, L140407 (2022).
- [10] Q. Ma, Y. Li, Y.-S. Choi, W.-C. Chen, S. J. Han, and C. L. Chien, Spin orbit torque switching of synthetic Co/Ir/Co trilayers with perpendicular anisotropy and tunable interlayer coupling, *Appl. Phys. Lett.* **117**, 172403 (2020).
- [11] C. C. Chiang, S. Y. Huang, D. Qu, P. H. Wu, and C. L. Chien, Absence of Evidence of Electrical Switching of the Antiferromagnetic Néel Vector, *Phys. Rev. Lett.* **123**, 227203 (2019).
- [12] Y. Li, D. Zheng, C. Liu, C. Zhang, B. Fang, A. Chen, Y. Ma, A. Manchon, and X. Zhang, Current-induced magnetization switching across a nearly room-temperature compensation point in an insulating compensated ferrimagnet, *ACS Nano* **16**, 8181 (2022).
- [13] X. Jia, K. Liu, K. Xia, and G. E. W. Bauer, Spin transfer torque on ferrimagnetic insulators, *Europhys. Lett.* **96**, 17005 (2011).
- [14] Q. Shao, C. Tang, G. Yu, A. Navabi, H. Wu, C. He, J. Li, P. Upadhyaya, P. Zhang, S. A. Razavi, Q. L. He, Y. Liu, P. Yang, S. K. Kim, C. Zheng, Y. Liu, L. Pan, R. K. Lake, X. Han, Y. Tserkovnyak, J. Shi, and K. L. Wang, Role of dimensional crossover on spin-orbit torque efficiency in magnetic insulator thin films, *Nat. Commun.* **9**, 3612 (2018).
- [15] O. J. Lee, L. Q. Liu, C. F. Pai, Y. Li, H. W. Tseng, P. G. Gowtham, J. P. Park, D. C. Ralph, and R. A. Buhrman, Central role of domain wall depinning for perpendicular magnetization switching driven by spin torque from the spin Hall effect, *Phys. Rev. B* **89**, 024418 (2014).
- [16] L. Zhu, D. C. Ralph, and R. A. Buhrman, Lack of Simple Correlation between Switching Current Density and Spin-Orbit-Torque Efficiency of Perpendicularly Magnetized Spin-Current-Generator-Ferromagnet Heterostructures, *Phys. Rev. Appl.* **15**, 024059 (2021).
- [17] L. Zhu, Switching of perpendicular magnetization by spin-orbit torque, *Adv. Mater.* (2023), doi: [10.1002/adma.202300853](https://doi.org/10.1002/adma.202300853).
- [18] L. Zhu, D. C. Ralph, and R. A. Buhrman, Maximizing spin-orbit torque generated by the spin Hall effect of Pt, *Appl. Phys. Rev.* **8**, 031308 (2021).
- [19] L. Zhu, L. Zhu, M. Sui, D. C. Ralph, and R. A. Buhrman, Variation of the giant intrinsic spin Hall conductivity of Pt with carrier lifetime, *Sci. Adv.* **5**, eaav8025 (2019).
- [20] J. W. Lee, Y.-W. Oh, S.-Y. Park, A. I. Figueroa, G. van der Laan, G. Go, K.-J. Lee, and B.-G. Park, Enhanced spin-orbit torque by engineering Pt resistivity in Pt/Co/ AlO_x structures, *Phys. Rev. B* **96**, 064405(2017).
- [21] R. J. Elliott, Theory of the effect of spin-orbit coupling on magnetic resonance in some semiconductors, *Phys. Rev.* **96**, 266 (1954).
- [22] Y. Yafet, g factors and spin-lattice relaxation of conduction electrons, *Solid State Phys.* **14**, 1 (1963).
- [23] J. Finley and L. Q. Liu, Spin-Orbit-Torque Efficiency in Compensated Ferrimagnetic Cobalt-Terbium Alloys, *Phys. Rev. Appl.* **6**, 054001 (2016).
- [24] J. Han, A. Richardella, S. A. Siddiqui, J. Finley, N. Samarth, and L. Liu, Room-Temperature Spin-Orbit Torque Switching Induced by a Topological Insulator, *Phys. Rev. Lett.* **119**, 077702 (2017).
- [25] P. Melchior, M. Rollinger, P. Thielen, S. Alebrand, U. Bierbrauer, C. Schneider, M. Gottwald, M. Hehn, S. Mangin, M. Cinchetti, and M. Aeschlimann, Energy-resolved magnetic domain imaging in TbCo alloys by valence band photoemission magnetic circular dichroism, *Phys. Rev. B* **88**, 104415 (2013).
- [26] T. Xu, Y. Cheng, Y. Dong, H. Bai, H.-A. Zhou, X. Shu, P. Gargiani, M. Valvidares, P. Yu, and W. Jiang, Evolution of Compensated Magnetism and Spin-Torque Switching in Ferrimagnetic $\text{Fe}_{1-x}\text{Tb}_x$, *Phys. Rev. Appl.* **19**, 034088 (2023).
- [27] Y. Tian, L. Ye, and X. Jin, Proper Scaling of the Anomalous Hall Effect, *Phys. Rev. Lett.* **103**, 087206 (2009).
- [28] L. J. Zhu, D. Pan, and J. H. Zhao, Anomalous Hall effect in epitaxial $\text{Li}_0\text{-Mn}_{1.5}\text{Ga}$ films with variable chemical ordering, *Phys. Rev. B* **89**, 220406(R) (2014).
- [29] D. Hou, G. Su, Y. Tian, X. Jin, S. A. Yang, and Q. Niu, Multi-variable Scaling for the Anomalous Hall Effect, *Phys. Rev. Lett.* **114**, 217203 (2015).
- [30] Y. Mimura, N. Imamura, and Y. Koshiro, Hall effect in rare-earth-transition-metal amorphous alloy Films, *J. Appl. Phys.* **47**, 3371 (1976).
- [31] P. Rajasekhar, K. Deepak Kumar, and G. Markandeyulu, Anomalous Hall effect studies on Tb-Fe thin films, *J. Magn. Mater.* **412**, 201 (2016).
- [32] S. Ota, P. V. Thach, H. Awano, A. Ando, K. Toyoki, Y. Kotani, T. Nakamura, T. Koyama, and D. Chiba, Strain-induced modulation of temperature characteristics in ferrimagnetic Tb-Fe films, *Sci. Rep.* **11**, 6237 (2021).
- [33] M. D. Davydova, P. N. Skirdkov, K. A. Zvezdin, J.-C. Wu, S.-Z. Ciou, Y.-R. Chiou, L.-X. Ye, T.-H. Wu, R. C. Bhatt, A. V. Kimel, and A. K. Zvezdin, Unusual Field Dependence of the Anomalous Hall Effect in Ta/Tb-Fe-Co, *Phys. Rev. Appl.* **13**, 034053 (2020).
- [34] X. P. Zhao, J. Lu, S. W. Mao, Z. F. Yu, H. L. Wang, X. L. Wang, D. H. Wei, and J. H. Zhao, $\text{Li}_0\text{-MnGa}$ based magnetic tunnel junction for high magnetic field sensor, *J. Phys. D: Appl. Phys.* **50**, 285002 (2017).
- [35] V. H. Babu, G. Markandeyulu, and A. Subrahmanyam, Effect of anisotropy on anomalous Hall effect in Tb-Fe thin films, *J. Appl. Phys.* **105**, 113907 (2009).
- [36] J. Delahaye, J. P. Brison, and C. Berger, Evidence for Variable Range Hopping Conductivity in the Ordered Quasicrystal $i\text{-AlPdRe}$, *Phys. Rev. Lett.* **81**, 4204 (1998).
- [37] T. Siegrist, P. Jost, H. Volker, M. Woda, P. Merkelbach, C. Schlockermann, and M. Wuttig, Disorder-induced localization in crystalline phase-change materials, *Nat. Mater.* **10**, 202 (2011).
- [38] C.-H. Lin and G. Y. Wu, Hopping conduction in granular metals, *Physica B* **279**, 341 (2000).
- [39] B. Abeles, P. Sheng, M. D. Coutts, and Y. Arie, Structural and electrical properties of granular metal films, *Adv. Phys.* **24**, 407 (1975).
- [40] N. F. Mott, The metal-insulator transition in extrinsic semiconductors, *Adv. Phys.* **21**, 785 (1972).
- [41] D. C. Ralph and R. A. Buhrman, Observations of Kondo Scattering without Magnetic Impurities: A Point Contact Study of

- Two-Level Tunneling Systems in Metals, *Phys. Rev. Lett.* **69**, 2118 (1992).
- [42] L. Zhu and J. H. Zhao, Anomalous resistivity upturn in epitaxial L_{21} - Co_2MnAl films, *Sci. Rep.* **7**, 42931 (2017).
- [43] T. Cichorek, A. Sanchez, P. Gegenwart, F. Weickert, A. Wojakowski, Z. Henkie, G. Auffermann, S. Paschen, R. Kniep, and F. Steglich, Two-Channel Kondo Effect in Glasslike ThAsSe , *Phys. Rev. Lett.* **94**, 236603 (2005).
- [44] L. J. Zhu, S. H. Nie, P. Xiong, P. Schlottmann, and J. H. Zhao, Orbital two-channel Kondo effect in epitaxial ferromagnetic L_{10} - MnAl films, *Nat. Commun.* **7**, 10817 (2016).
- [45] L. Zhu, G. Woltersdorf, and J. Zhao, Observation of orbital two-channel Kondo effect in a ferromagnetic L_{10} - MnGa film, *Sci. Rep.* **6**, 34549 (2016).
- [46] G. Záránd, Existence of a two-channel Kondo regime for tunneling impurities with resonant scattering, *Phys. Rev. B* **72**, 245103 (2005).
- [47] G. T. Meaden, Conduction electron scattering and the resistance of the magnetic elements, *Contemp. Phys.* **12**, 313 (1971).
- [48] F. Wu, E. P. Sajitha, S. Mizukami, D. Watanabe, T. Miyazaki, H. Naganuma, M. Oogane, and Y. Ando, Electrical transport properties of perpendicular magnetized Mn-Ga epitaxial films, *Appl. Phys. Lett.* **96**, 042505 (2010).
- [49] J. M. Ziman, A theory of the electrical properties of liquid metals. I: The monovalent metals, *Philos. Mag.* **6**, 1013 (1961).
- [50] S. R. Nagel, Temperature dependence of the resistivity in metallic glasses, *Phys. Rev. B* **16**, 1694 (1977).
- [51] L. J. Zhu, S. H. Nie, and J. H. Zhao, Anomalous Hall effect in L_{10} - MnAl films with controllable orbital two-channel Kondo effect, *Phys. Rev. B* **93**, 195112 (2016).
- [52] D. Hou, Y. Li, D. Wei, D. Tian, L. Wu, and X. Jin, The anomalous Hall effect in epitaxial face-centered-cubic cobalt films, *J. Phys.: Condens. Matter* **24**, 482001 (2012).
- [53] L. Ye, Y. Tian, X. Jin, and D. Xiao, Temperature dependence of the intrinsic anomalous Hall effect in nickel, *Phys. Rev. B* **85**, 220403(R) (2012).
- [54] M. Chen, Z. Shi, W. J. Xu, X. X. Zhang, J. Du, and S. M. Zhou, Tuning anomalous Hall conductivity in $L_{10}\text{FePt}$ films by long range chemical ordering, *Appl. Phys. Lett.* **98**, 082503 (2011).
- [55] G. Su, Y. Li, D. Hou, X. Jin, H. Liu, and S. Wang, Anomalous Hall effect in amorphous $\text{Co}_{40}\text{Fe}_{40}\text{B}_{20}$, *Phys. Rev. B* **90**, 214410 (2014).
- [56] N. Kiyohara, T. Tomita, and S. Nakatsuji, Giant Anomalous Hall Effect in the Chiral Antiferromagnet Mn_3Ge , *Phys. Rev. Appl.* **5**, 064009 (2016).